Biomaterials 180 (2018) 52–66

Contents lists available at ScienceDirect

Biomaterials

journal homepage: www.elsevier.com/locate/biomaterials

Engineering innervated secretory epithelial organoids by magnetic three-dimensional bioprinting for stimulating epithelial growth in salivary glands

Christabella Adine [a], Kiaw K. Ng [a], Sasitorn Rungarunlert [b], Glauco R. Souza [c, d], João N. Ferreira [a, e, f, *]

[a] Faculty of Dentistry, National University of Singapore, Singapore
[b] Department of Preclinical and Applied Animal Science, Faculty of Veterinary Science, Mahidol University, Nakhon Pathom, 73170, Thailand
[c] University of Texas Health Sciences Center at Houston, Houston, TX, USA
[d] Nano3D Biosciences Inc., Houston, TX, USA
[e] Faculty of Dentistry, Chulalongkorn University, Bangkok, Thailand
[f] National Institute of Dental and Craniofacial Research, National Institutes of Health, Bethesda, MD, USA

ARTICLE INFO

Article history:
Received 22 March 2018
Received in revised form
8 June 2018
Accepted 9 June 2018
Available online 12 June 2018

Keywords:
Bioprinting
Magnetic nanoparticles
Organoids
Salivary gland
Radiotherapy
Xerostomia

ABSTRACT

Current saliva-based stimulation therapies for radiotherapy-induced xerostomia are not fully effective due to the presence of damaged secretory epithelia and nerves in the salivary gland (SG). Hence, three-dimensional bio-engineered organoids are essential to regenerate the damaged SG.

Herein, a recently validated three-dimensional (3D) biofabrication system, the magnetic 3D bioprinting (M3DB), is tested to generate innervated secretory epithelial organoids from a neural crest-derived mesenchymal stem cell, the human dental pulp stem cell (hDPSC). Cells are tagged with magnetic nanoparticles (MNP) and spatially arranged with magnet dots to generate 3D spheroids. Next, a SG epithelial differentiation stage was completed with fibroblast growth factor 10 (4–400 ng/ml) to recapitulate SG epithelial morphogenesis and neurogenesis. The SG organoids were then transplanted into *ex vivo* model to evaluate their epithelial growth and innervation.

M3DB-formed spheroids exhibited both high cell viability rate (>90%) and stable ATP intracellular activity compared to MNP-free spheroids. After differentiation, spheroids expressed SG epithelial compartments including secretory epithelial, ductal, myoepithelial, and neuronal. Fabricated organoids also produced salivary α-amylase upon FGF10 stimulation, and intracellular calcium mobilization and trans-epithelial resistance was elicited upon neurostimulation with different neurotransmitters. After transplantation, the SG-like organoids significantly stimulated epithelial and neuronal growth in damaged SG.

It is the first time bio-functional innervated SG-like organoids are bioprinted. Thus, this is an important step towards SG regeneration and the treatment of radiotherapy-induced xerostomia.

1. Introduction

Saliva plays an important role in oral homeostasis, which includes balancing a neutral pH, lubricating the oral cavity, protecting against foreign stimuli (bacteria, virus, etc), and aiding in food digestion [1–3]. Salivary gland (SG) hypofunction accompanied with a subjective feeling of dry mouth (or xerostomia) is a clinical condition whereby saliva output is greatly reduced [4], causing discomfort during mastication and speech [5]. Radiotherapy (RT) for head and neck cancers (HNC) and several other systemic conditions (e.g. Sjögren's syndrome, anemia) can result in xerostomia. In HNC patients, the therapeutic alleviation of xerostomia is difficult to achieve due to the RT-induced damage inflicted in the secretory epithelial and neuronal compartments [6,7]. Bio-engineering such innervated secretory tissues *in vitro* for potential clinical replacement and/or regeneration has become paramount [8–10].

* Corresponding author. Faculty of Dentistry, Chulalongkorn University, 54 Henri-Dunant Road, Pathumwan, Bangkok 10330, Thailand.
E-mail addresses: christabella.adine@u.nus.edu (C. Adine), kiawkiaw.ng@gmail.com (K.K. Ng), sasitorn.run@mahidol.edu (S. Rungarunlert), gsouza@n3dbio.com (G.R. Souza), Joao.F@chula.ac.th (J.N. Ferreira).

https://doi.org/10.1016/j.biomaterials.2018.06.011
0142-9612/

Approaches with cellularized three-dimensional (3D) tissue constructs have been a promising therapeutic option to generate *in vitro* SG spheroids, micro-tissues or organoids [6,8,9,11–15]. Ogawa and colleagues [10] reported a fetal bioengineered SG can be generated by a cell recombination protocol containing epithelium, mesenchyme, neurons and endothelium. The entire fetal organ could be transplanted into adult mice, reconnect with the existing ductal system and function properly [10]. This strategy revealed some potential for clinical translation. However, it required available fetal tissues and their cellular progenitors, which are not available "off-the-shelf" in humans.

More recently, researchers started a Phase 1 clinical trial to investigate the use of adipose-derived mesenchymal stem cells (MSC) for SG replacement [16], since several MSC types showed in the past encouraging outcomes in SG regeneration [17,18]. To this end, adult stem cell-based 3D cultures for biofabrication have been utilized as a supportive strategy for the recapitulation of organ development and morphogenesis [19,20], and particularly towards SG repair and regeneration [6,15,17,21,22]. The 3D culture systems are rapidly superseding the 2D as they better mimic physiologic conditions and maintain appropriate cell-cell and cell-matrix interactions [23]. The majority of reported 3D culture systems utilizes nonhuman-derived substrates (e.g. Matrigel) [8,13,24,25], which limits their potential for clinical use. Complex hydrogel biomimetic scaffolds can constitute an alternative, though the size of each fabricated 3D tissue construct in hydrogels is limited (<300 μm in diameter) and these constructs require a long culture period (4 months) [11]. Hydrogels have also been combined with basement membrane proteins such as elastin [26], laminins [27], and others [14], some of which raised immunogenicity and tumorigenesis concerns [27–29]. In the last decade, organ- and cell-based bioprinting have been emerging as promising bio-engineering/biofabrication approaches for hydrogels and scaffold-free constructs [30–32]. To simplify the biofabrication of these bioengineered tissue/organoids, a scaffold-free culture platform is proposed herein where a magnetic 3D bioprinting (M3DB) approach is utilized to promptly produce 3D spheroids. This recent M3DB biofabrication process allows for 3D cellular spatial arrangement and spheroid formation within less than 24 h, and facilitates spheroid handling and transferring as well as high-throughput analysis and imaging [6,33]. In this culture platform, cells in monolayer are magnetized with a magnetic nanoparticle cocktail consisting of gold, iron oxide, and poly-L-lysine, after which they are directed into a 3D spheroid using mild magnetic forces into magnet dots [33]. As cells rearrange and interact to find an equilibrium size from which to grow long-term, spheroids immediately start to shorten in diameter [34]. Cells are then allowed to build their own 3D microenvironment and extracellular matrix. Further, the magnetic nanoparticles used in this culture platform support cell proliferation and metabolism, without increasing pro-inflammatory and oxidative stress [33], and have shown biocompatibility and negligible immune response after transplantation [35].

Hence, the aims of this study were: (1) to generate an innervated secretory epithelial organoid from a human MSC cell type using an *in vitro* M3DB biofabrication process and (2) to assess the epithelial growth/regenerative potential after transplantion in irradiated and healthy SG *ex vivo* models. A neural crest-derived MSC, the human dental pulp stem cell (hDPSC), was selected. This cell line has the same embryological origin as SG-derived stem cells from the primitive oral ectoderm, which can generate SG epithelial [21] and neuronal lineages [36]. After SG epithelial differentiation with key SG development cues, such as fibroblast growth factor 10, the M3DB-formed spheroids expressed different SG-specific epithelial and neuronal cell compartments like an organotypic culture. The ultimate goal was to bioengineer a SG organoid with innervation and bio-functional properties resembling the function of the SG acinar secretory unit for the future purpose of clinical transplantation.

2. Materials and methods

2.1. Adult stem cell source

Human dental pulp stem cells (hDPSCs) were commercially obtained from AllCells (Alameda, CA, USA) from three different donors. These stem cells were derived from the pulp tissues of exfoliated deciduous teeth, primary incisors, or permanent third molar teeth. Cells (up to passage 6) were cultured in Dulbecco's Modified Eagle Medium (DMEM) with 1% Glutamax, 10% fetal bovine serum and 1% antibiotic-antimycotic in the presence of a humidified environment (37 °C, 5% CO_2). Media was changed every other day. To maintain their undifferentiated state, cells were passaged at 75–80% confluency and their surface markers were consistently assessed by flow cytometry. All materials and general culture reagents were purchased from Gibco (Thermo Fisher Scientific, USA), and all chemicals were purchased from Sigma-Aldrich (MO, USA) unless otherwise specified.

2.2. Characterization of hDPSC phenotype

hDPSCs were passaged and dissociated using TrypLE (Gibco) and viable single cells were counted using the Trypan Blue exclusion method (Thermo Fisher Scientific). Total viable cell counts were determined and the population doubling time (PDT) of hDPSC was calculated up to passage 6 using the following formula, PDT (hours) = (Culture time (hours) x log (2))/(log (total number of viable harvested cells - log (total number of viable seeded cells)).

A minimum of 5×10^5 cells was used for each tube for flow cytometry analysis. Single cells were blocked in MACS buffer (Miltenyi Biotec, Germany). Conjugated primary antibodies were added at predetermined optimal concentrations as per Supplementary Table 1 and incubated at 4 °C for 20 mins. For intracellular staining, cells were fixed with fresh 4% paraformaldehyde (PFA) at room temperature (RT) for 20 mins and followed by permeabilization with 0.05% Triton-X/MACS buffer. Next, incubation was done with Pacific Blue anti-Ki67 antibody for 1 h at 4 °C. Then, cells were washed three times with MACS buffer and resuspended in the same buffer for flow cytometry analysis. The respective isotype IgG control was used in parallel at the same concentration as their corresponding primary antibodies. Analysis was performed using LSR Fortessa™ cell analyzer (BD Bioscience, USA), and data were analyzed by FlowJo software (Tree Star, USA). Gating was performed using unstained cells or isotype IgG stained control cells. The percentage of cells that were specifically and positively stained with the antibody/surface marker was plotted in a graph. All experiments were conducted with hDPSCs between passage 3 and 6 based on the consistent expression of pro-mitotic, hDPSC, hMSC and SG progenitor markers.

2.3. Spheroid formation stage with M3DB platform

The magnetic nanoparticle used in the spheroid formation stage is a solution of gold and iron oxide nanoparticles crosslinked by a biopolymer named poly-L-lysine. These nanoparticle solution has been comprehensively described in Refs. [37,38].

hDPSC were prepared for bioprinting via M3DB according to this Biofabrication methodology [33] with a few modifications (see Fig. 1 flowchart). Briefly, confluent hDPSC (75–80% confluency) were statically incubated overnight (~12 h) with magnetic

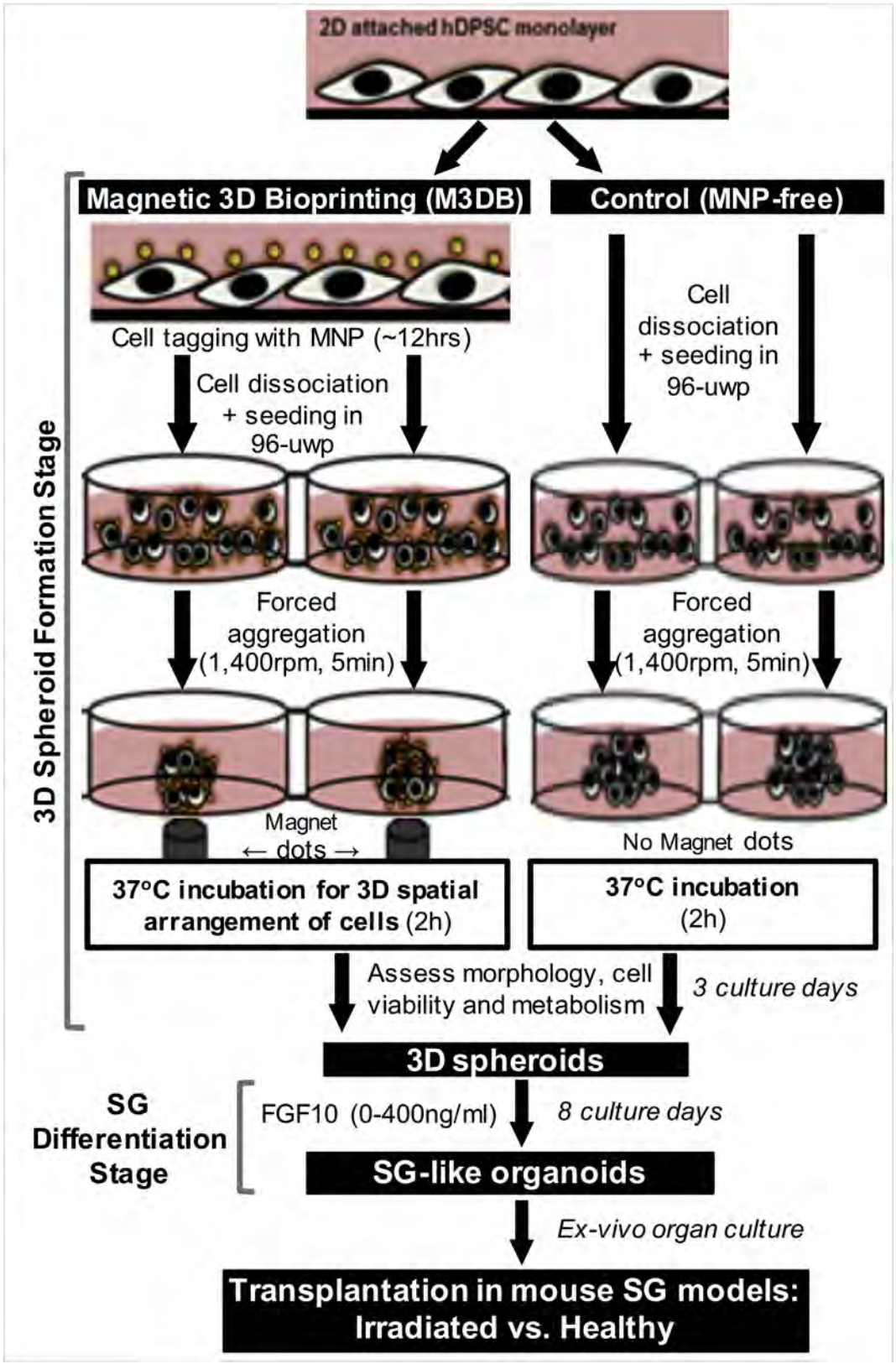

Fig. 1. Flowchart with the Biofabrication methodological steps required towards the formation and SG differentiation stages of 3D spheroids towards SG-like organoids for transplantation purposes by using M3DB or a Control 3D *in vitro* culture platforms. MNP: magnetic nanoparticles; uwp: ultra-low attachment well plate. FGF10: Fibroblast growth factor 10. h: hours.

nanoparticles (NanoShuttle, Nano3D Biosciences, Houston, TX, USA) at a concentration of 1 μL/2.5 × 10^4 cells (40 pg/cell) to allow for cell tagging to render them magnetic properties. Subsequently, magnetized cells were gently washed and enzymatically detached with TrypLE, resuspended in growth media, then seeded into ultra-low attachment 96-well plates (Corning, USA) at a concentration of 3 × 10^6 cells/well. Forced aggregation employing gravitational force with centrifugation at 1400 rpm for 5 mins was then performed to facilitate cell clustering at the bottom of the well. A magnetic pin drive of 96 neodymium magnets (0.0625″ OD, Nano3D Biosciences) was placed below the 96-well plate to assemble the cells into spheroids at the bottom of the well. The physical characteristics of the dot magnets used have been described in detail elsewhere [33]. These spheroids were bio-printed over the magnet dots for 15 min. After 1–2 h, the plate was removed from the magnet dots, and spheroids were allowed to grow their cell numbers for 1–7 days during the "3D spheroid formation stage". Note that the diameter of the spheroids decrease with increased cell viability as crucial cell-cell interactions take place to form the extracellular matrix [33]. A similar 3D culture system to M3DB but without magnetic nanoparticles (MNP-free) for cell tagging, was used as a "Control" 3D culture system to compare with M3DB (Fig. 1) [39]. The morphology and size of hDPSC spheroids derived from different culture systems were assessed by taking bright field and phase-contrast micrographs at different magnifications with a DMi8 fluorescent microscope with automated *xy* platform and *z*-staking (Leica Microsystems, Germany). To quantify the diameter size, spheroids were scanned with a high resolution Perfection V550 Epson flatbed scanner with 6,400dpi optical resolution (Seiko Epson Corporation, Japan).

2.4. Real-time propidium iodide-based cell viability assays

To measure hDPSC cell viability in real-time during the 3D spheroid formation stage in the M3DB system, a ReadyProbes® Cell Viability Kit (Blue/Red, Invitrogen, ThermoFisher Scientific, USA) was used according to manufacturer instructions. Briefly, 2 drops of each reagent (propidium iodide and NucBlue® Live) was added to 1 mL of media containing the spheroids. Viability was determined by quantifying the number of total (blue-stained) versus non-viable cells with compromised plasma membrane integrity (pinkish red-stained) using the DMi8 fluorescence microscope (Leica Microsystems) with automated z-stacking. A conventional "Control" 3D culture system (similar to M3DB but MNP-free) was used as a control system to compare with M3DB. ImageJ software (Bethesda, NIH, USA) with a cell count plugin was used to calculate fluorescence intensity of viable and non-viable cells.

2.5. Intracellular ATP luciferase-based cytotoxicity assays

To quantify metabolically active hDPSC in spheroids formed M3DB and Control culture systems during the "3D spheroid formation" stage, a ATP luciferase-based cell cytotoxicity assay for 3D microtissues (CellTiter-Glo® 3D, Promega) was conducted over a period of 72 h (3 days) with 2 × 10^4 cells/well, following the manufacturer protocol. Bioluminescence was measured with a Glomax® luminometer (Promega). All values were subtracted from average background bioluminescence values from wells with media containing no cells to calculate the final relative luminescence.

2.6. Salivary epithelial and neuronal differentiation of hDPSC

During the spheroid formation stage, after hDPSC reached the highest cell viability (>90% after 3 days via M3DB), the SG epithelial differentiation stage was initiated. To drive the hDPSC differentiation towards creating a committed epithelial cellular compartment in the spheroid, the growth media was first changed to an epithelial differentiation media (EDM) composed of defined keratinocyte serum-free media (Gibco) supplemented with an early cue to initiate SG development, all-trans-retinoic acid 5 μM (Sigma, USA) as per previous optimizations and publications [6,40]. Spheroids previously treated with RA (5–10 μM) upregulated SG progenitor genes (*krt5* and *krt14*) and produced high levels of α-amylase compared with untreated control. After culture day 3, to further recapitulate SG late development and epithelial morphogenesis, the above EDM media was supplemented with fibroblast growth factor-10 (FGF10, R&D systems, MN, USA) between 0 and 400 ng/ml for 5 days [41]. Media was changed every day. The entire differentiation stage lasted 8 culture days after the initial 3-day spheroid formation stage. To produce control neurospheres (enriched with neurons), hDPSC were treated with neurogenic differentiated media as previously reported [42]. This media was composed of L-glutamine-enriched DMEM and neurobasal medium with N2 and 10% FBS. Neurosphere cultures were run for 8 days like spheroids for SG differentiation.

2.7. Gene expression assays

To quantify mRNA expression levels on hDPSC 2D monolayer cultures through different passages, on undifferentiated hDPSC and on SG differentiated hDPSC spheroids, quantitative PCR was performed. Briefly, total RNA was extracted from cell lysates and then treated with DNAse using Ambion MicroRNA kit (ThermoFisher Scientific Inc., USA) according to manufacturer's protocol. The purity and concentration of extracted total RNA were determined by Nanodrop ND1000 (Thermo Fisher, USA). Next, cDNA was synthesized from total RNA by reverse transcriptase enzyme iScript® (Bio-Rad, USA) and diluted to 1 ng/μl. The qPCR reaction was done in a total volume of 20 μl consisting 10 μl cDNA, 9.5 μl iTaq® (Bio-Rad, USA), 0.5 μl of forward and reverse primer mix in a Bio-Rad CFX96 system. Data was analyzed by $2^{-(ddCT)}$ method to calculate relative expression of target genes compared to reference gene *s29*. The oligonucleotide sequences of both forward and reverse primers are listed in Supplementary Table 2.

2.8. Immunocytochemistry and protein assays

Undifferentiated hDPSC and differentiated spheroids were fixed in 4% paraformaldehyde for 1 min at RT and washed with PBS thrice. After removal of PBS, spheroids were incubated with 0.5% Triton X (Sigma) in PBS for 15 min at RT to allow antibody permeabilization and washed with 0.05% Tween20 (Sigma) in PBS. Spheroids were blocked with 10% donkey serum (Sigma), 5% BSA (Sigma), in 0.1% Tween20/PBS for 2 h with continuous shaking at RT to reduce background. The cells were then washed 3 times with 0.1% Tween20/PBS and incubated with primary antibody for overnight at 4 °C with a continuous shaking. Primary antibodies and their dilutions are listed on Supplementary Table 1. For secondary antibody labelling, the cells were washed thrice with PBS and incubated with Alexa Fluor 488, 594, 647 secondary antibodies (Invitrogen, Thermo Fisher Scientific) for 40–60 min at RT. All spheroids were also counterstained with a nuclear dye (Hoechst 33342, 1:1000, Invitrogen) for 5 min at RT with continuous shaking. The specimens were rinsed with PBS three times with shaking and mounted onto glass slides. Evaluation of the specimens was performed by using both fluorescent, confocal, and multiphoton microscopes: DMi8 (Leica Microsystems, Germany), Zeiss LSM 710 (Zeiss, Germany), and a Leica TCS SP8 DM6000 CFS upright confocal with a two-photon laser-scanning microscope (Leica Microsystems), respectively. Sequential 5 μm z-stack images were

acquired through the spheroids using the confocal microscopes above, and 3D images were rendered along the x- and y-axis as well as maximum intensity projections.

Ex vivo transplanted tissues were immunostained using the above described protocol with β3-tubulin, Sox2, and Ki67 primary antibodies and counterstained with a nuclear dye. Series of *z*-stack images were taken using Olympus FV1000 (Olympus Corporation, Japan) and images were evaluated with Imaris (BitPlane, USA). Area of β3-tubulin$^+$ cells was measured with surface detection algorithm and normalized to the total volume of the salivary glands. The number of Ki67$^+$ cells was quantified using "dots detection" algorithm with 5 μm estimated nuclear diameter size inclusion and filtered by their intensity.

2.9. Salivary amylase enzymatic assays

During the SG differentiation stage of hDPSC spheroids, α-amylase activity in the conditioned media was assessed using the EnzChek Ultra Amylase Assay Kit (Invitrogen) as an indicator of SG secretory function. To measure α-amylase secretion after carbachol stimulation (10 μM), conditioned media were collected at day 11 of differentiation culture. The activity of this enzyme was determined following the manufacturer protocols by measuring the fluorescent signal after excitation at 495 nm with a microplate reader (Tecan Group Ltd, Switzerland). Appropriate starch standards were used to generate a standard curve and experimental values were subtracted to background fluorescent values from unconditioned media (without cells).

2.10. Intracellular calcium influx

The influx of calcium towards intracellular compartments can trigger secretory activities, and therefore is usually used as a readout for epithelial secretory function upon autonomic neurostimulation (parasympathetic and sympathetic). To determine calcium mobilization in cells in the final organoids upon neurostimulation, muscarinic and adrenergic agonists were added to the conditioned media with the organoids after completion of the SG differentiation stage. To measure and visualize the calcium influx, a Fluo-4 direct calcium assay (Invitrogen) was used according to the manufacturer protocol. Calcium chloride was first added to spheroid culture, and 18 h afterwards they were stimulated with a cholinergic/muscarinic agonist, Carbachol (10–1000 μM). The adrenergic agonist Isoproterenol (10–1000 μM) was added 24 h after calcium chloride. Calcium intracellular mobilization and fluorescence intensity was determined by using time-lapse imaging as set by the LAS X software on a Leica DMi8 fluorescence microscope. Sequential image acquisition was performed every 5 s per cycle.

2.11. Trans-epithelial electrical resistance

SG differentiated spheroids were transferred into transwell polyester membrane filters (Corning, USA) using a magnetic pen (Nano3D Biosciences). Trans-epithelial electrical resistance (TEER) generated by epithelial polarization was measured in four separate SG differentiated spheroids, using an EMD Millipore Millicell-ERS2 Volt-Ohm Meter (Fisher Scientific, Thermo Fisher Scientific). Negative controls with transwell filters and without spheroids were used to measure background TEER values, which were then subtracted from readings obtained from transwell filters containing spheroid cultures. Probe measurements were taken in different locations (at least 3) until the values stabilize within 5 s. Then, all measurements taken at consistent locations in each well were averaged. Furthermore, to ensure that the temperature does not fluctuate (fluctuation will affect TEER measurements), TEER readings were done within 5 min after removal from the incubator at 37 °C.

2.12. Transmission electron microscopy

For ultrastructural analysis of inter-cellular tight junctions, subcellular secretory vesicles and MNPs, differentiated M3DB-based spheroids were fixed with 3% glutaraldehyde and 2% paraformaldehyde in PBS buffer for electron microscopy. Spheroid tissues were rinsed in PBS for 15 min at 4 °C. Post-fixation was performed in 1% osmium tetroxide (Sigma) in the same buffer solution at 4 °C for 2 h, and tissues were dehydrated in a graded series of alcohol and embedded in resin. Semi-thin sections were obtained using glass knives with Ultracut E Microtome (Leica Microsystems), and ultra-fine sections (90–100 nm) were mounted on copper grids of 100 meshes. The grids were stained by 0.4% lead citrate and examined in a JEM-1010 transmission electron microscope (JEOL, USA) adjusted to 80 kV. Primary salivary gland cell cultures were used as positive controls.

2.13. Magnetic nanoparticle release profile in in vitro cultures

Following removal of magnet dots from the culture plates, plates with hDPSC spheroids are scanned with a Perfection V550 Epson flatbed scanner (Epson, USA) for up to 29 days of culture to generate high resolution coloured images of the spheroid (6,400dpi). Since MNP possess an intrinsic dark brown colour, the area filled by MNP in each spheroid/well was quantified using Image J software (NIH) as well as the total area of the spheroid in each well. The cumulative MNP release at different culture time points was calculated by using this formula: (1−(MNPs area/Total spheroid area)) x 100%.

2.14. Mouse SG models for transplantation studies

Salivary gland (SG) explants (including both submandibular and sublingual glands) were dissected from ICR mouse embryos at embryonic day 13 and cultured as previously described [43]. Briefly, all SG were placed in polycarbonate porous filters in 35 mm culture dishes and incubated with DMEM/F-12 (Gibco) serum-free fresh medium containing 1% penicillin/streptomycin, transferrin and vitamin C. The treatment groups were the following: (1) irradiation model (IR), (2) transplanted with SG organoid after irradiation (IR + SG organoid), non-irradiation model (nonIR), transplanted with SG organoid in non-irradiation model (nonIR + SG organoid). After 8 h of culture, to develop the IR SG model, SGs were irradiated in a BIOBEAM 8000 gamma irradiator (Gamma-Service Medical GmBH, Germany) with a single dose of irradiation (7Gy). Afterwards, all glands were cultured further for 3 more days. Explants were imaged at baseline, day 1, 2 and 3 in bright field at 4–10x magnification using a Leica M80 stereomicroscope with a MC120 HD colour camera. The epithelial bud numbers were counted using Image J cell counter in a blinded fashion after stripping all treatment labels from all images. This counting was performed by an independent researcher not directly involved in this research project. Epithelial growth index was calculated at the different time points by normalizing the bud number at that time point to the baseline, and by further dividing it to the irradiated control treatment (IR control). All treatment groups used 5–6 SG pairs.

The National University of Singapore Institutional Animal Care and Use Committee (NUS IACUC) has ethically approved all animal experiments under the protocol number R14-306. This work was performed at all times in compliance with the ARRIVE guidelines and the National Institutes of Health guide for the care and use of laboratory animals (NIH Publications No. 8023, revised 1978).

2.15. Statistical analysis

All experiments were replicated at least two times. Student's *t*-test was used to determine differences among two independent experimental groups. Paired Student's *t*-tests were run to compare differences through culture time. One-way analysis of variance (ANOVA) followed by Dunnett's post-hoc tests were used for multiple comparisons among more than two groups. The significance level was set at an alpha value of 0.05. GraphPad Prism version 6 (GraphPad Software Inc., CA, USA) was used to perform all statistical analyses.

3. Results

3.1. Human DPSCs are enriched in specific SG epithelial progenitors before spheroid culture

An initial immunophenotypic characterization of hDPSC cells was performed to validate their hMSC-like and hDPSC-like phenotype as well as determine the presence of pro-mitotic cells and putative SG epithelial progenitors. Flow cytometry revealed that hDPSC were positive for hMSC standard surface markers CD73, CD90, and CD105 as previously reported [44,45], and their expression was retained up to passage 6 (Supplementary Fig. 1). Further, more than 70% of the hDPSC population was pro-mitotic ($Ki67^+$) through P6, and more than 90% of hDPSCs expressed putative SG markers CD29 and CD90, and limited expression of CD24 and c-Kit (or CD117) (Fig. 2A). Likewise, human SG-derived primary cells also have high expression of CD29 and CD90 markers, and low c-Kit expression patterns [46–48]. Such markers are also present in epithelial progenitor/stem cells capable of forming SG organoids [15,47,49]. Taken together, these findings indicate the suitability of hDPSC as a potential cell source towards our goal of modeling the SG epithelia.

3.2. M3DB system supported the consistent biofabrication of 3D spheroids with high hDPSC viability rate

To generate viable and consistent size-controlled 3D hDPSC spheroids, we used the M3DB biofabrication culture system and thoroughly evaluated the spheroids for size, morphology, cell viability and metabolic activity (Fig. 2B–E). The M3DB culture was compared to a MNP-free Control 3D culture to produce spheroids (Fig. 1). Spheroid-like cell aggregates are observed immediately after 15 mins (after removal of magnet dots), whereas the Control took longer time to form homogenous and compact spheroids (24–48 h) (Fig. 2B). M3DB-formed spheroids exhibited a consistent morphology with no loss of cell aggregation for up to 7 days (Fig. 2B). On the other hand, control spheroids started to break apart after 3 days of culture. The spheroid diameter shortened sharply as expected within the first 3 days due to early cell-cell interactions (Fig. 2B–C, Supplementary Fig. 2), but diameter remained constant thereafter. A large number of viable cells (>90%) is present in the M3DB-formed spheroid during the first 3 days, which further confirmed the biocompatibility of MNP in M3DB (Fig. 2C–D). Further, M3DB supported an intracellular ATP activity in spheroids comparable to that of Control culture (Fig. 2E). Cell *adherens* junctions (E-cadherin and EpCAM) between hDPSCs were prominent through the spheroid periphery and core, thereby tightly packing cells and providing an epithelium-like appearance (Supplementary Fig. 2). The high cell viability outcomes and the stability of spheroid size after 3 culture days provided the rationale to implement a 3-day spheroid formation stage before SG differentiation was initiated.

3.3. M3DB supported the formation of SG-like epithelial spheroids

Following the 3D spheroid formation stage with the M3DB biofabrication process, the spheroid was subjected to a differentiation stage to recapitulate SG development for 8 days. All end product SG differentiated hDPSC-derived spheroids exhibited consistent diameter sizes at millimetre-level (ranging from 0.96 to 1.28 mm), regardless of FGF10 stimulation (Fig. 3A). The number of SG ductal epithelial and myoepithelial cell types ($KRT5^+$, $KRT14^+$) significantly increased with FGF10 media stimulation (Figs. 3B and 4A). Epithelial secretory ($AQP5^+$) cells were present as well at high levels (75–90%) (Figs. 3 and 4A-B). Gene expression assays and immunoblots have further confirmed these phenotypic findings (Fig. 4C and data not shown). Further, FGF10 stimulation on the M3DB culture induced increasing levels of basal α-amylase enzymatic activity, significant at 40 and 400 ng/ml in the 3D spheroid (Fig. 4D). In addition, differentiated spheroids were poorly vascularized as per low PECAM-1/$CD31^+$ cell numbers (Supplementary Fig. 3). The limited number of pluripotent cells ($SOX2^+$) found after SG differentiation confirmed the presence of differentiated cellular phenotypes in the spheroid (Supplementary Fig. 3).

3.4. SG differentiated spheroids had bio-functional innervation

SG differentiated spheroids contained a neuronal cell compartment with 15–40% β3-$tubulin^+$ cells, regardless of FGF10 stimulation (Fig. 5A, Supplementary Fig. 4). The presence of a large neuronal network was observed after immunocytochemistry of SG differentiated spheroids (Fig. 5B). Upon media neurostimulation with parasympathetic and sympathetic neurotransmitters (Carbachol and Isoproterenol, respectively) at different concentrations (10–1000 μM), intracellular calcium mobilization is elicited in differentiated spheroids (Fig. 6C–F).

In summary, the recapitulation of SG development in hDPSC-derived M3DB cultures consistently generated 3D spheroids with SG acinar and ductal epithelial, and neuronal compartments. Such spheroids were similar to organotypic milimetre-scale tissues or organoids.

3.5. Differentiated spheroids displayed a polarized secretory epithelia

Next, an ultrastructural tissue analysis was conducted in SG differentiated spheroids to evaluate epithelial cell polarization. SG spheroids presented a polarized secretory epithelia (epithelial cell displaying secretory granules) with lumenized compartments and tight junction structures between epithelial cells (Fig. 6A). The presence of this highly organized polarized epithelial compartment defined an epithelial barrier in the SG spheroids, which elicited a significant trans-epithelial electrical resistance ($p < 0.05$) upon different salivary autonomic neurotransmitters (Fig. 6B).

Taken together, these findings indicate that these tissue organoids have a SG-like polarized epithelial compartment and neuro-epithelial functional properties, which may allow an unidirectional flow of saliva mimicking therefore the normal SG secretory unit.

3.6. Cells in differentiated spheroids held limited numbers of MNP

The release of MNP was quantified in M3DB cultures with SG differentiated spheroids. After 11 culture days, there was approximately 47 ± 10% of cumulative release of MNP to the media

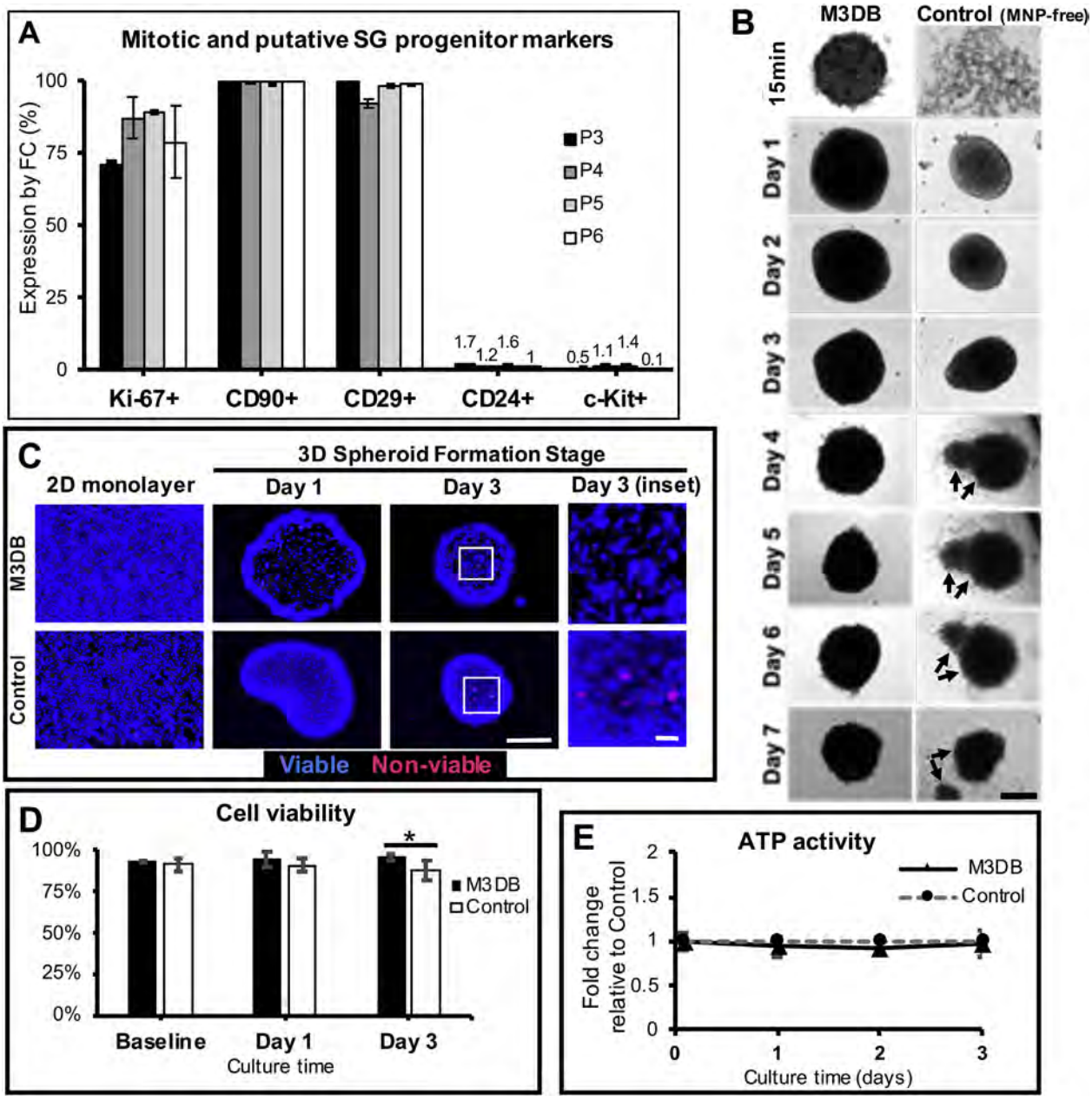

Fig. 2. M3DB culture platform supported the consistent formation of 3D spheroids and the maintenance of high numbers of viable hDPSCs. (A) Expression by flow cytometry of mitotic and putative SG-specific progenitor markers in populations of hDPSC in 2D monolayers before the initiation of the 3D spheroid formation stage (M3DB). FC: flow cytometry. Additional data for 2D cultures with expression of hMSC surface markers in Supplementary Fig. 1. **(B)** Representative bright field microscopy images of the 3D spheroids during the formation stage via M3DB and Control cultures showing spheroid breakdown starting at day 4 in the Control (MNP-free) system (black arrows). Baseline images were taken 15 min after magnet removal. Mag.: 5X. Scale bar: 200 μm **(C)** Representative images of 3D spheroids formed by M3DB and Control systems with fluorescently-labeled viable cells (blue) and membrane-compromised non-viable cells (pink/red) using a real-time cell viability kit. Scale bar: 200 μm and insets 100 μm. **(D)** Quantification of viable and non-viable cells. N = 4–5. Data are means ± SD and were subjected to a Student's *t*-test: $^{*}p < 0.05$ when comparing M3DB versus Control. **(E)** Quantification of intracellular ATP activity in spheroids formed by M3DB relative to Control by luciferase-based assays. Additional data for this figure with size quantification of spheroids through 3-day culture in Supplementary Fig. 2. (For interpretation of the references to colour in this figure legend, the reader is referred to the Web version of this article.)

(Fig. 7A). Such spheroids were then evaluated at the ultrastructural level on the TEM. The remaining MNP were not present within the cells or in the plasma membranes after 11 days, as they were rather observed sparsely throughout the extracellular matrix (Fig. 7B). Moreover, in long-term M3DB cultures (after 29 days), the levels of MNP in spheroids were minimal (cumulative release rate: 92 ± 4%, Fig. 7A). Overall, these outcomes indicate a remarkable low potential for detrimental effects of MNP on cellular viability and metabolism.

3.7. Transplantation of SG organoids stimulated epithelial growth and innervation

After transplantation of SG-like organoids into the excretory ductal area of developing SG glands *ex-vivo*, organoids significantly rescued epithelial growth on our acute SG fetal models of irradiation (Fig. 8A–B). In healthy SG models, the transplantation of SG organoids also strikingly stimulated the epithelial growth of the glands (Fig. 8A–B). There was also an prominent increase in

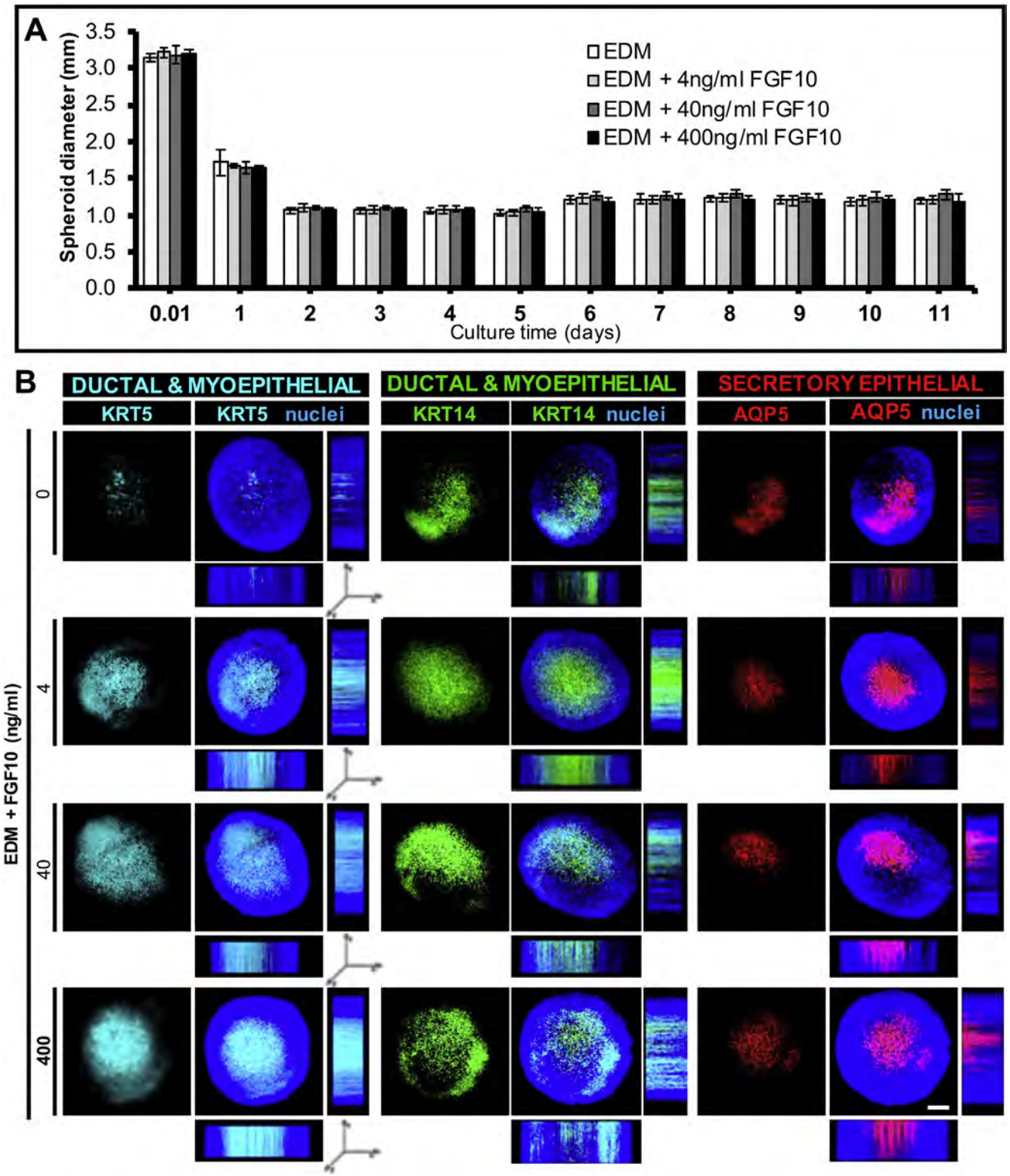

Fig. 3. Spheroids formed by M3DB after SG differentiation stage expressed different SG epithelial cell compartments with FGF10 stimulation. (A) Quantification of the spheroid diameter during the entire culture (11 days) with different concentrations of FGF10 stimulations in the media. N = 8. Data are means ± SD. EDM: epithelial differentiation media. **(B)** Representative fluorescent images of the differentiated spheroids immunostained with different SG epithelial markers: ductal and myoepithelial (KRT5, KRT14), and acinar secretory epithelial (AQP5). Images shown are maximum intensity projections with their XYZ orthogonal projections at the right side and below. Mag.:10X. Scale bar: 200 μm. EPI: epithelial. Additional data for this figure with other markers (for vascularization and multipotency) is in Supplementary Fig. 3.

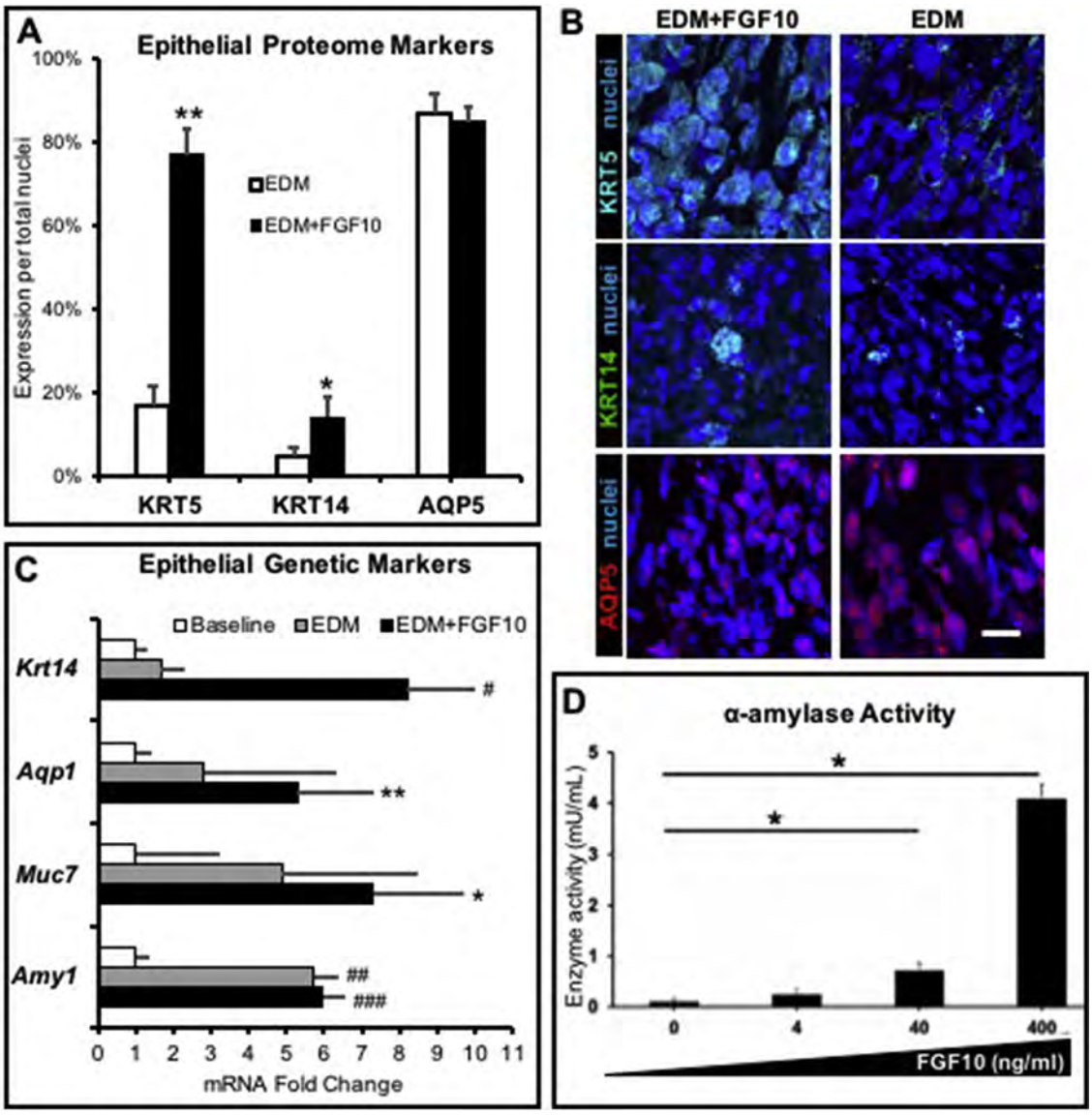

Fig. 4. Expression of SG-specific epithelial markers at proteome and transcriptome levels and salivary α-amylase activity on spheroids after SG differentiation stage. (A) Quantification of SG epithelial(acinar, ductal and myoepithelial) markers on spheroids by measuring the fluorescence intensity of the target marker and normalizing to total nuclei. Data are mean ± SD and Student's *t*-test was performed: $^{*}p < 0.05$, $^{**}p < 0.0001$ when compared with no FGF10. **(B)** Representative cells from spheroids after completion of the SG differentiation stage without and with FGF10 (400 ng/ml) treatments are immunostained with ductal epithelial and myoepithelial markers (KRT5 and KRT14) and acinar markers (AQP5). Mag.: 40X. Scale bar: 20 μm. **(C)** Differentiated spheroids expressing SG secretory acinar epithelial and myoepithelial genes. Fold change values are normalized to the housekeeping gene *s29* and compared to undifferentiated spheroids at baseline. All other spheroid groups are differentiated with EDM for 8 days with 400 ng/ml of FGF10. N = 3–10. Data are presented as means ± SEM. Fold change is analyzed using Student's *t*-test: $^{*}p = 0.08$, $^{**}p = 0.06$, $\#p < 0.05$, $\#\#p < 0.001$ and $\#\#\#p<0.0001$ all compared to spheroids at baseline (before differentiation stage is initiated). **(D)** α-amylase enzymatic activity on the spheroids treated with increasing concentrations of FGF10. N = 4. Data are means ± SEM and one-way analysis of variance (ANOVA) with post-hoc Dunnett's test is performed: $^{*}p < 0.05$ when compared with no FGF10 treatment.

proliferative cells ($SOX2^{+}$, $Ki67^{+}$) after transplantation of the organoid, particularly in the epithelia of IR SG compared to its respective IR control, at both acinar and ductal epithelial compartments (Fig. 8C, Supplementary Fig. 5). This was not though with statistical significance as per embryogenesis-driven biological variation (Supplementary Fig. 6).

Moreover, the neuronal network/compartment of the *ex vivo* gland and the SG-like organoids were integrated after transplantation (Fig. 8C). This network was significantly dense in the treatment groups when compared to controls (Supplementary Fig. 6).

Lastly, proliferative cell compartments were present in both the center and periphery of SG-like organoids after transplantation indicating they retain a regenerative potential (Supplementary Fig. 7).

4. Discussion

No feasible 3D biofabrication process exists to engineer an innervated human SG *in vitro* [8,9]. Several 3D bio-engineering systems have successfully demonstrated the ability of primary SG epithelial cells to self-assemble and exhibit polarization properties on artificial scaffolds incorporating SG basement membrane molecules [9,11–15,26]. Despite such achievements, the resulting tissues/organoids do not support the development of a neuronal network within the epithelial tissues. Innervation is deemed crucial

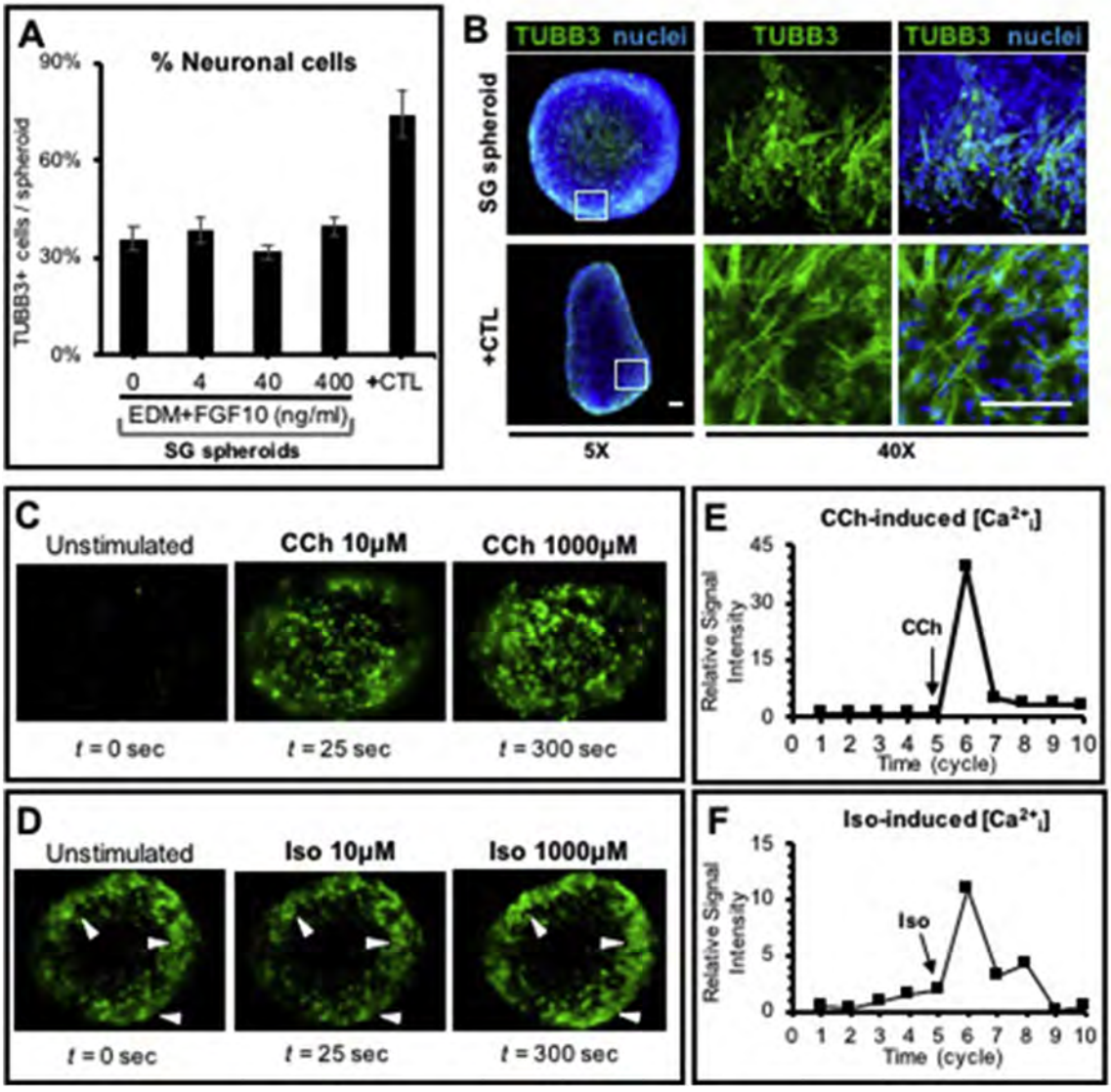

Fig. 5. SG differentiated spheroids were innervated and responsive to cholinergic and adrenergic neurotransmitters. (A) Quantification of neurons immuno-reactive to anti-β3-tubulin pan-neuronal antibody in spheroids after the SG differentiation stage. N = 4. Data are means ± SD and are normalized to total nuclei in each spheroid. Data were analyzed using one-way analysis of variance with post-hoc Dunnett's test: there was no difference between EDM-enriched groups with FGF10 0–400 ng/ml +CTL: neuronal 3D cultures (neurospheres). **(B)** Representative images of SG differentiated spheroids (stimulated with FGF10 400 ng/ml) immunostained for nerves (TUBB3) and counterstained with a nuclear dye. Images are maximum intensity projections of the entire spheroid on the left. White frame denotes insets for the higher magnification (40x) images on the far right. Scale bar: 100 µm **(C–D)** Representative microscopy time-lapsed images showing calcium ion [Ca^{2+}_i] mobilization in SG spheroid real time cultures after calcium fluorescence labeling (in green) before and after: **(C)** cholinergic stimulation with Carbachol (CCh) and **(D)** adrenergic stimulation with Isoproterenol (Iso). Mag.: 10x. **(E–F)** Intracellular calcium influx in SG spheroids during **(E)** stimulation with CCh 10 µM and **(F)** stimulation with Iso 10 µM. Data are representative of 3–4 biological spheroids and are presented as a relative signal intensity where each reading was normalized to baseline calcium influx (at unstimulated state). (For interpretation of the references to colour in this figure legend, the reader is referred to the Web version of this article.)

to maintain and/or repair SG epithelial secretory cells and restore saliva flow after radiotherapy damage as reported in our previous work [43] and by other colleagues [50].

Herein, our hDPSC-derived M3DB process offered an important step towards producing innervated and bio-functional SG-like organoids *in vitro*. Such innervated secretory epithelia secreted salivary amylase (Fig. 5C–D) and was responsive to both cholinergic (parasympathetic) and β-adrenergic (sympathetic) neurotransmitters (Fig. 6C–E and 7B). Lastly and more importantly, the SG-like organoid rescued epithelial growth in the irradiated SG model, and stimulated innervation in the irradiated and healthy glands after *ex vivo* transplantation with neuronal integration arising from both organ and transplant (Fig. 8).

For an effective SG organ formation, the "ideal" scaffold requires a complex set of tunable chemical cues and mechanical and topographical properties with different tissue compliances [12,26]. As a result, this "ideal" scaffold requires complex functionalization and biofabrication processes, and the end product is perhaps difficult to achieve. Conversely, scaffold-free bio-engineered platforms using 3D bioprinting of magnetized cells can facilitate a prompt cell clustering in 3D as well as cell-cell interactions to allow cells to generate a tightly-packed epithelia to ultimately become a functional organ [6,37,38]. With M3DB, the 3D arrangement of cells based on the shape and position of magnet dots are termed as bioprinting, and can occur in normal and ultra-low attachment culture plates [33]. M3DB can be used as a culture aid/platform or

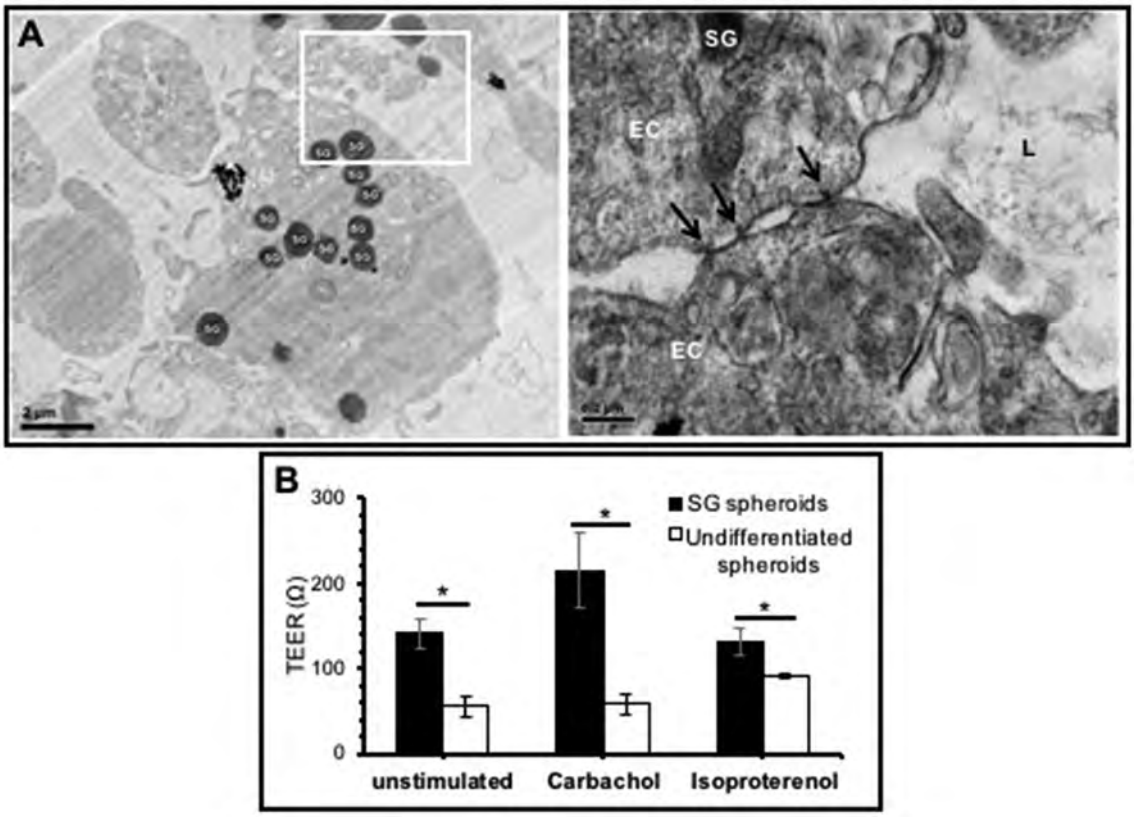

Fig. 6. SG differentiated spheroids are composed of polarized secretory epithelial cells creating a trans-epithelial barrier. (A) Transmission electron microscope micrographs of spheroids differentiated after EDM+FGF10 400 ng/ml media supplementation. Epithelial cells (EC) with multiple electron-dense secretory granules (SG, left micrograph) are interacting through intercellular tight junction structures (black arrows, right micrograph) and creating a lumen (L). Right micrograph corresponds to an inset of a magnified area from the white frame on the left. Mag.: 6,000X (left), 50,000X (right). **(B)** Trans-epithelial electrical resistance in SG differentiated spheroids versus undifferentiated spheroids before and after stimulation with Carbachol (10 μM) and Isoproterenol (10 μM). N = 3–4. Data are presented as means ± SEM and were analyzed using a Student's *t*-test: $^{*}p < 0.05$ when comparing both spheroids.

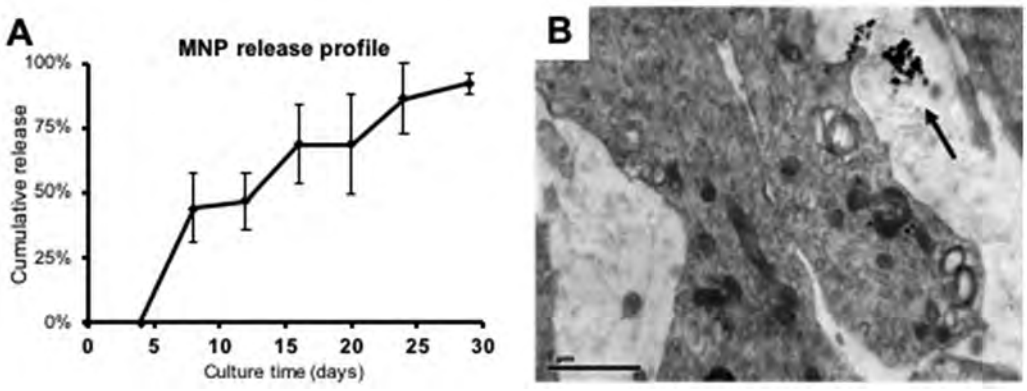

Fig. 7. Magnetic nanoparticles were continuously released from cells to the media and to the extracellular matrix during long-term culture. (A) Release profile of magnetic nanoparticles (MNP) per spheroid in the M3DB system through long-term culture. Data are presented as means ± SD (N = 8). **(B)** Micrograph taken by transmission electron microscopy showing the presence of MNPs (black arrow) in the extracellular matrix of organoids after completion of the differentiation stage (culture day 11). Mag.: 20,000X.

as a bioprinting tool that can consistently control the size of the spheroids by tuning the concentration of MNP, cell number, and the size of the magnet dots [6]. Moreover, together with laser-based bioprinting and other bioprinting and/or bioassembly methods [31,51], M3DB aids in the cell patterning while also being a good source of bioink in the extrusion approach (ongoing unpublished work).

During our spheroid formation stage, cells positioned as 3D aggregates during the first 15 mins of culture (after magnet removal), and maintained a consistent uniform spheroid-like shape from culture day 3 through 11 (Fig. 2B–C and 3A). As expected, there was an early diameter size reduction (from 15 mins to day 3 of culture) most probably due to robust cell-cell interactions and epithelial cell packing (Supplementary Fig. 2), also seen in our previous studies [6,33]. After 3 days, the fluctuations in spheroid size were stable and controlled. Cytotoxicity of the magnetic

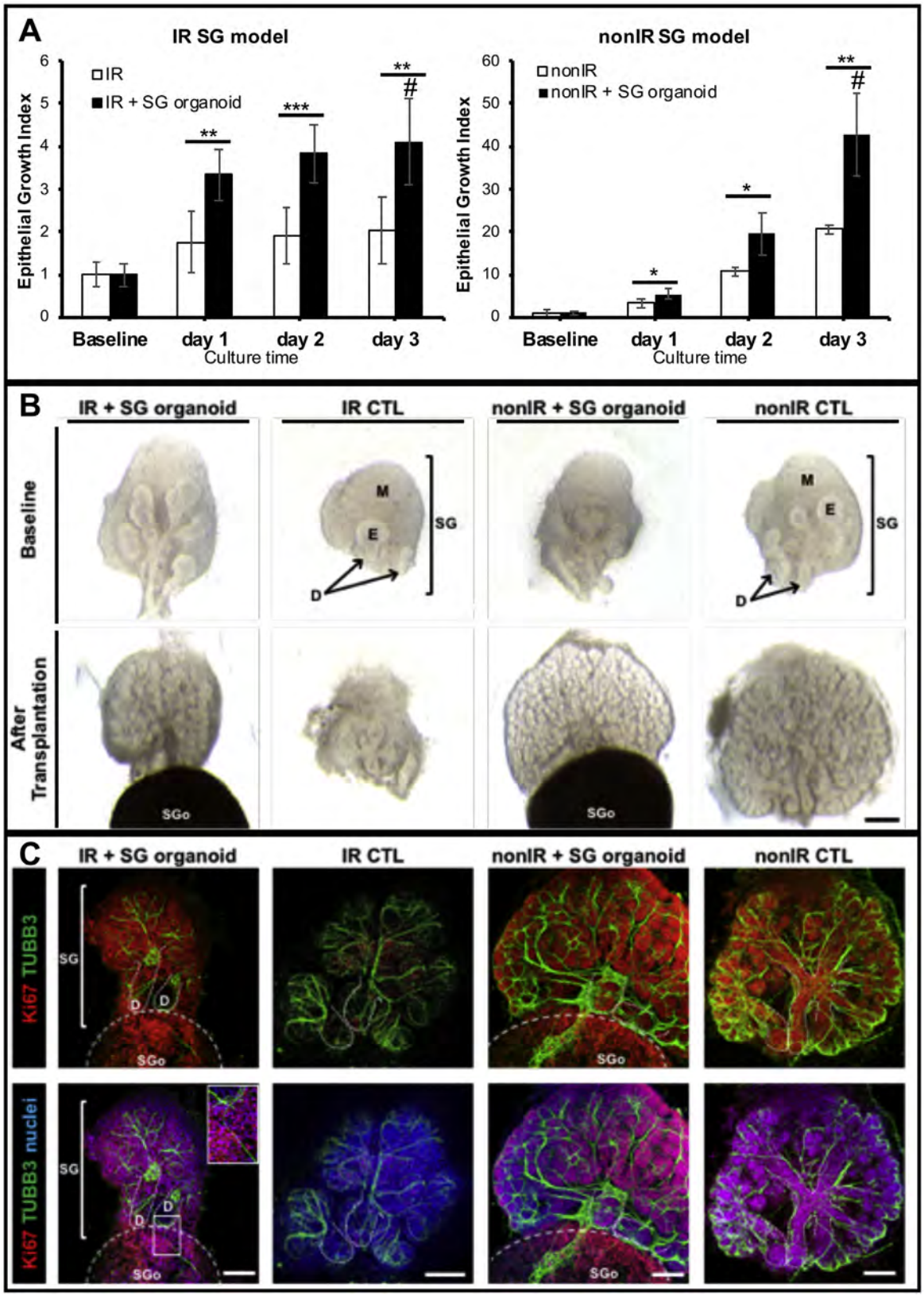

Fig. 8. Epithelial growth and innervation was significantly stimulated after transplantation of SG-like organoids in mouse SG. (A) Epithelial growth index of SG after transplantation in irradiated (IR, left graph) and healthy (non-irradiated or nonIR, right graph) SG *ex vivo* models. Data are presented as means ± SD (N = 5–6). Unpaired and paired Student's *t*-tests with Welch's correction were performed: $^{*}p < 0.05$, $^{**}p < 0.01$, $^{***}p < 0.001$ when comparing both groups; $\#p<0.001$ when comparing baseline with endpoint. **(B)** Bright field images acquired from each SG at baseline and at the last endpoint of the transplantation stage. Mag.: 4X. Scale bar: 200 μm. IR: irradiated. nonIR: non-irradiated. M: mesenchyme. E: Epithelial bud. D: Ducts. **(C)** Representative images of mouse SG immunostained for nerves (TUBB3), proliferative epithelial cells (Ki67) and counterstained with a nuclear dye. Images are maximum intensity projections of the entire spheroid on the left. Inset: close up view of innervation integration between SGo and SG. SG: salivary glands (submandibular and sublingual). SGo: salivary gland-like organoid. Dotted white line denotes the SG ducts. Dashed white line denotes the perimeter of the SG-like organoid. Scale bar: 200 μm.

nanoparticles (MNP) was negligible in the M3DB system with viability, ATP metabolism being similar to MNP-free 3D Control cultures (Fig. 2C–E). Further, the cumulative release of MNP from spheroids to media *in vitro* was quite fast and steady during long-term cultures (Fig. 7A). This significantly restricts the potential for detrimental effects on cellular biocompatibility and genotoxicity. This limited cytotoxicity has been observed in previous reports, whereby MNP supported viable and proliferative cells in 3D spheroids [37]. More importantly, these MNP were successfully used in *in vivo* stem cell therapies to treat nerve injuries and further possessed promising biocompatibility outcomes with a negligible immune response after transplantation [35]. Despite this, the immune response will still need to be confirmed in other SG transplantation models *in vivo*.

Studies on fetal SG organogenesis have shown the key role of FGF10 in SG development and morphogenesis [52–54]. In our studies, upon stimulation with FGF10, the spheroids (formed by M3DB) had larger SG-like epithelial cell compartments ($KRT5^+$, $KRT14^+$, $AQP5^+$ cells) as well as higher levels of salivary α-amylase activity when concentrations of FGF10 increased (Fig. 4A–D). In addition, differentiated spheroids exhibited a neuronal compartment (Fig. 5A–B), though vascularization was limited (Supplementary Fig. 3).

Despite our findings with this adult stem cell line (hDPSC), autologous SG-derived epithelial stem/progenitor cells are still considered an ideal cell source for modeling the SG epithelia. However, these autologous cells have limited availability and poor expansion capabilities and cannot generate a functional neuronal compartment (innervation) [8,11,15]. Primary SG cells in 3D floating cultures have poor cell growth rates even in long-time cultures, requiring larger biopsies to have a clinically relevant transplant [6,8]. This is unpractical as the donor usually has limited healthy SG tissue after radiotherapy [8]. For this reason, we focused herein on a known adult stem cell line capable of generating epithelial and neuronal lineages in 3D platforms. Recently, a study demonstrated that adult stem cells derived from human dental follicle could differentiate into functional SG cells in the presence of a 3D Matrigel scaffold [21]. Despite the promising outcomes, the differentiation process involved a long culture period (25–28 days) and a xenogeneic scaffold, thereby limiting clinical translation. In our generated tissue organoids, a SG-like organotypic structure was present with a well-packed polarized epithelia holding prominent cell *adherens* and TJs and several intracellular secretory vesicles with lumenized areas at the ultrastructural level (Fig. 6A, Supplementary Fig. 2). Hence, this organoid structure mimicked the complex epithelial secretory acini architecture present in the human SG. Additionally, organoids carried a neuronal network, and exhibited SG-like epithelial secretory functions upon different parasympathetic and sympathetic neuro-stimulations. The presence of a neuronal compartment can be in part due to the formation of neuronal lineages seen in studies with differentiated hDPSC [42,44]. Other recent SG engineering studies have fabricated SG-like micro-tissues co-assembled with both epithelial and myoepithelial compartments [9]. This latter study was a major breakthrough, however the final tissues lacked innervation and were not robust in size (<100 μm in diameter) to recapitulate the large secretory acinar compartments seen in the native human SG. The milimeter-level organoids generated in our study are remarkable but can pose technical challenges in terms of nutrient and oxygen diffusion and upon analysing or imaging biological mechanisms as a 3D SG *in vitro* model. Confocal and multi-photon microscopy with multiple detector systems through the spheroid allowed us to provide more biological assessments into the inner cellular core of the organoid. Several proliferative cell compartments were present in both the center and periphery of SG-like organoids after transplantation (Supplementary Fig. 7). Also, the SG-like organoids could be visualized for intracellular calcium mobilization upon the stimulation with different neurotransmitters at a wide range of concentrations (10–1000 μM, Fig. 6C–F), and a trans-epithelial electrical barrier was enhanced as well after different neuro-stimulations (Fig. 6B). This trans-epithelial barrier is essential in a polarized secretory epithelia to mimic the unidirectional flow of saliva, a phenomenon that requires the presence of TJs. At ultrastructural level, organoids possessed TJ structures packing the secretory epithelial cells. Hence, this M3DB bio-engineered culture platform with hDPSCs generated a bio-functional polarized epithelia with innervation. Despite this, an apicobasal polarization was challenging to determine due to tightly packed epithelial cells, and vascularization was limited in the organoids. This latter finding is possibly due to low haematopoietic subpopulations in hDPSC capable of generating $CD31^+$ cells. However, this can potentially be achieved in future studies with endothelial cell co-cultures with hDPSC and proper stimulation for angiogenesis [55].

More importantly, upon transplantation, the SG organoids stimulated epithelial growth in both irradiated-damaged SG and healthy glands (Fig. 8A–B). Additionally, both neuronal networks coming from the SG and SG-like organoid merged, thus providing an indication of potential integration of neuronal networks in future *in vivo* studies. The epithelial proliferation and innervation rescue in the damaged SG was achieved upon transplantation of 1 SG organoid. Therefore, in an autologous stem cell transplantation strategy, this would be a feasible cell number to work with as per the eventually limited cell sources or cell availability in clinical scenario (where elderly patients with xerostomia may have limited number of hDPSC due to the limited number of teeth). Furthermore, we believe this biological effect is not dependent on pluripotent stem cells since $SOX2^+$ cells were scarce in the organoids (Supplementary Fig. 3) limiting the potential for cell immortality and tumorigenesis. Nevertheless, this study successfully bioprinted an innervated SG-like organoid with relevant bio-functional secretory epithelia capable of stimulating robust epithelial growth after transplantation in damaged and healthy SG.

5. Conclusions

This study describes for the first time a bioprinting process (M3DB) that promptly and consistently fabricates robust spheroids and enables the formation of innervated bio-functional tissue organoids with different SG-like cellular compartments. Upon transplantation, these SG-like organoids significantly stimulated the epithelial and neuronal growth in irradiation damaged and healthy SG models. This SG-like organoid model can be used as tool for drug cytotoxicity screening and mechanistic studies. More importantly, further studies will test the regenerative potential of these organoids in long-term/chronic radiotherapy-induced xerostomia models in both small and large animal models.

Authors competing interests statement

The authors have no competing interests except for G.R.S. The University of Texas M.D. Anderson Cancer Center (UTMDACC) and Rice University, together with their researchers, have filed patents on the technology and intellectual property reported here. G.R.S. has equity in Nano3D Biosciences, Inc. UTMDACC and Rice University manage the terms of these arrangements in accordance with their established institutional conflict-of-interest policies.

Acknowledgments

This work was supported by the National Medical Research

Council in Singapore [grant number: NMRC/CNIG/1131/2015], and Chulalongkorn University in Thailand to J.F. Funding from Mahidol University in Thailand [grant numbers: E04/2560 and 114/2560] was provided to S.R. We would like to give thanks to Ms. Phoebe Castillo and Ms. Adeline Koh for their support in troubleshooting cell culture experimental set ups with the M3DB culture platform, and to Dr. Yusuf Ali and Mr. Riasat Hasan for generously providing access to the multiphoton microscope facility.

Appendix A. Supplementary data

Supplementary data related to this article can be found at https://doi.org/10.1016/j.biomaterials.2018.06.011.

References

[1] A.M. Diaz-Arnold, C.A. Marek, The impact of saliva on patient care A literature review, J. Prosthet. Dent 88 (3) (2002) 337–343.
[2] O. Grundmann, G.C. Mitchell, K.H. Limesand, Sensitivity of salivary glands to radiation: from animal models to therapies, J. Dent. Res. 88 (10) (2009) 894–903.
[3] P. de Almeida, A. Grégio, M. Machado, A. Soares de Lima, L. Azevedo, Saliva composition and functions: a comprehensive review, J. Contemp. Dent. Pract. 9 (3) (2008) 72–80.
[4] C. Hong, J.N.A.R. Ferreira, Salivary hypofunction in aging adults, in: J.N.A.R. Ferreira, J. Fricton, N. Rhodus (Eds.), Orofacial Disorders: Current Therapies in Orofacial Pain and Oral Medicine, Springer International Publishing, Cham, 2017, pp. 105–112.
[5] S.B. Jensen, A.M.L. Pedersen, A. Vissink, E. Andersen, C.G. Brown, A.N. Davies, J. Dutilh, J.S. Fulton, L. Jankovic, N.N.F. Lopes, A.L.S. Mello, L.V. Muniz, C.A. Murdoch-Kinch, R.G. Nair, J.J. Napeñas, A. Nogueira-Rodrigues, D. Saunders, B. Stirling, I. von Bültzingslöwen, D.S. Weikel, L.S. Elting, F.K.L. Spijkervet, M.T. Brennan, A systematic review of salivary gland hypofunction and xerostomia induced by cancer therapies: prevalence, severity and impact on quality of life, Support. Care Canc. 18 (8) (2010) 1039–1060.
[6] J.N. Ferreira, S. Rungarunlert, G. Urkasemsin, C. Adine, G.R. Souza, Three-dimensional bioprinting nanotechnologies towards clinical application of stem cells and their secretome in salivary gland regeneration, Stem Cell. Int. 2016 (2016), 7564689.
[7] Y.H. Chan, T.W. Huang, T.H. Young, P.J. Lou, Human salivary gland acinar cells spontaneously form three-dimensional structures and change the protein expression patterns, J. Cell. Physiol. 226 (11) (2011) 3076–3085.
[8] I. Lombaert, M.M. Movahednia, C. Adine, J.N. Ferreira, Concise review: salivary gland regeneration: therapeutic approaches from stem cells to tissue organoids, Stem Cell. 35 (1) (2017) 97–105.
[9] T. Ozdemir, P.P. Srinivasan, D.R. Zakheim, D.A. Harrington, R.L. Witt, M.C. Farach-Carson, X. Jia, S. Pradhan-Bhatt, Bottom-up assembly of salivary gland microtissues for assessing myoepithelial cell function, Biomaterials 142 (2017) 124–135.
[10] M. Ogawa, T. Tsuji, Reconstitution of a Bioengineered Salivary Gland Using a Three-dimensional Cell Manipulation Method, Current Protocols in Cell Biology, John Wiley & Sons, Inc, 2001.
[11] P.P. Srinivasan, V.N. Patel, S. Liu, D.A. Harrington, M.P. Hoffman, X. Jia, R.L. Witt, M.C. Farach-Carson, S. Pradhan-Bhatt, Primary Salivary Human Stem/Progenitor Cells Undergo Microenvironment-driven Acinar-like Differentiation in Hyaluronate Hydrogel Culture, Stem Cells Translational Medicine, 2016.
[12] S.B. Peters, N. Naim, D.A. Nelson, A.P. Mosier, N.C. Cady, M. Larsen, Biocompatible tissue scaffold compliance promotes salivary gland morphogenesis and differentiation, Tissue Eng. 20 (11–12) (2014) 1632–1642.
[13] O.M. Maria, A. Zeitouni, O. Gologan, S.D. Tran, Matrigel improves functional properties of primary human salivary gland cells, Tissue Eng. 17 (9–10) (2011) 1229–1238.
[14] H.S. Shin, Y.M. Kook, H.J. Hong, Y.M. Kim, W.G. Koh, J.Y. Lim, Functional spheroid organization of human salivary gland cells cultured on hydrogel-micropatterned nanofibrous microwells, Acta Biomater. 45 (2016) 121–132.
[15] S. Pringle, M. Maimets, M. van der Zwaag, M.A. Stokman, D. van Gosliga, E. Zwart, M.J. Witjes, G. de Haan, R. van Os, R.P. Coppes, Human salivary gland stem cells functionally restore radiation damaged salivary glands, Stem Cell. 34 (3) (2016) 640–652.
[16] C. Gronhoj, D.H. Jensen, P.V. Glovinski, S.B. Jensen, A. Bardow, R.S. Oliveri, L. Specht, C. Thomsen, S. Darkner, K. Kiss, A. Fischer-Nielsen, C. von Buchwald, First-in-man mesenchymal stem cells for radiation-induced xerostomia (MESRIX): study protocol for a randomized controlled trial, Trials 18 (1) (2017) 108.
[17] O.M. Maria, S.D. Tran, Human mesenchymal stem cells cultured with salivary gland biopsies adopt an epithelial phenotype, Stem Cell. Dev. 20 (6) (2011) 959–967.
[18] Y. Sumita, Y. Liu, S. Khalili, O.M. Maria, D. Xia, S. Key, A.P. Cotrim, E. Mezey, S.D. Tran, Bone marrow-derived cells rescue salivary gland function in mice with head and neck irradiation, Int. J. Biochem. Cell Biol. 43 (1) (2011) 80–87.
[19] H. Clevers, Modeling development and disease with organoids, Cell 165 (7) (2016) 1586–1597.
[20] K. Kretzschmar, H. Clevers, Organoids: modeling development and the stem cell niche in a dish, Dev. Cell 38 (6) (2016) 590–600.
[21] Q.L. Xu, A. Furuhashi, Q.Z. Zhang, C.M. Jiang, T.H. Chang, A.D. Le, Induction of salivary gland-like cells from dental follicle epithelial cells, J. Dent. Res. 96 (9) (2017) 1035–1043.
[22] S. Pringle, R. Van Os, R.P. Coppes, Concise review: adult salivary gland stem cells and a potential therapy for xerostomia, Stem Cell. 31 (4) (2013) 613–619.
[23] J.J. Campbell, C.J. Watson, Three-dimensional culture models of mammary gland, Organogenesis 5 (2) (2009) 43–49.
[24] O.M. Maria, O. Maria, Y. Liu, S.V. Komarova, S.D. Tran, Matrigel improves functional properties of human submandibular salivary gland cell line, Int. J. Biochem. Cell Biol. 43 (4) (2011) 622–631.
[25] N.J. Leigh, J.W. Nelson, R.E. Mellas, A.D. McCall, O.J. Baker, Three-dimensional cultures of mouse submandibular and parotid glands: a comparative study, J. Tissue Eng. Regen. Med. 11 (3) (2017) 618–626.
[26] Z.I. Foraida, T. Kamaldinov, D.A. Nelson, M. Larsen, J. Castracane, Elastin-PLGA hybrid electrospun nanofiber scaffolds for salivary epithelial cell self-organization and polarization, Acta Biomater. 62 (2017) 116–127.
[27] K. Nam, C.L. Maruyama, C.S. Wang, B.G. Trump, P. Lei, S.T. Andreadis, O.J. Baker, Laminin-111-derived peptide conjugated fibrin hydrogel restores salivary gland function, PLoS One 12 (11) (2017), e0187069.
[28] E. Delamarre, S. Taboubi, S. Mathieu, C. Berenguer, V. Rigot, J.C. Lissitzky, D. Figarella-Branger, L. Ouafik, J. Luis, Expression of integrin alpha6beta1 enhances tumorigenesis in glioma cells, Am. J. Pathol. 175 (2) (2009) 844–855.
[29] K. Nam, C.S. Wang, C.L.M. Maruyama, P. Lei, S.T. Andreadis, O.J. Baker, L1 peptide-conjugated fibrin hydrogels promote salivary gland regeneration, J. Dent. Res. 96 (7) (2017) 798–806.
[30] V. Mironov, R.P. Visconti, V. Kasyanov, G. Forgacs, C.J. Drake, R.R. Markwald, Organ printing: tissue spheroids as building blocks, Biomaterials 30 (12) (2009) 2164–2174.
[31] J.M. Lee, W.Y. Yeong, Design and printing strategies in 3D bioprinting of cell-hydrogels: a review, Adv. Healthc. Mater. 5 (22) (2016) 2856–2865.
[32] J. Groll, T. Boland, T. Blunk, J.A. Burdick, D.W. Cho, P.D. Dalton, B. Derby, G. Forgacs, Q. Li, V.A. Mironov, L. Moroni, M. Nakamura, W. Shu, S. Takeuchi, G. Vozzi, T.B. Woodfield, T. Xu, J.J. Yoo, J. Malda, Biofabrication: reappraising the definition of an evolving field, Biofabrication 8 (1) (2016), 013001.
[33] H. Tseng, J.A. Gage, T. Shen, W.L. Haisler, S.K. Neeley, S. Shiao, J. Chen, P.K. Desai, A. Liao, C. Hebel, R.M. Raphael, J.L. Becker, G.R. Souza, A spheroid toxicity assay using magnetic 3D bioprinting and real-time mobile device-based imaging, Sci. Rep. 5 (2015) 13987.
[34] D.M. Timm, J. Chen, D. Sing, J.A. Gage, W.L. Haisler, S.K. Neeley, R.M. Raphael, M. Dehghani, K.P. Rosenblatt, T.C. Killian, H. Tseng, G.R. Souza, A high-throughput three-dimensional cell migration assay for toxicity screening with mobile device-based macroscopic image analysis, Sci. Rep. 3 (2013) 3000.
[35] H. Lin, N. Dhanani, H. Tseng, G.R. Souza, G. Wang, Y. Cao, T.C. Ko, H. Jiang, R. Wang, Nanoparticle improved stem cell therapy for erectile dysfunction in a rat model of cavernous nerve injury, J. Urol. 195 (3) (2016) 788–795.
[36] M. Takahashi, T. Suzawa, A. Yamada, T. Yamaguchi, K. Mishima, N. Osumi, K. Maki, R. Kamijo, Identification of gene expression profile of neural crest-derived cells isolated from submandibular glands of adult mice, Biochem. Biophys. Res. Commun. 446 (2) (2014) 481–486.
[37] G.R. Souza, J.R. Molina, R.M. Raphael, M.G. Ozawa, D.J. Stark, C.S. Levin, L.F. Bronk, J.S. Ananta, J. Mandelin, M.-M. Georgescu, J.A. Bankson, J.G. Gelovani, T.C. Killian, W. Arap, R. Pasqualini, Three-dimensional tissue culture based on magnetic cell levitation, Nat. Nanotechnol. 5 (4) (2010) 291–296.
[38] W.L. Haisler, D.M. Timm, J.A. Gage, H. Tseng, T.C. Killian, G.R. Souza, Three-dimensional cell culturing by magnetic levitation, Nat. Protoc. 8 (10) (2013) 1940–1949.
[39] J.R. Ferreira, R. Padilla, G. Urkasemsin, K. Yoon, K. Goeckner, W.S. Hu, C.C. Ko, Titanium-enriched hydroxyapatite-gelatin scaffolds with osteogenically differentiated progenitor cell aggregates for calvaria bone regeneration, Tissue Eng. 19 (15–16) (2013) 1803–1816.
[40] D.M. Wright, D.E. Buenger, T.M. Abashev, R.P. Lindeman, J. Ding, L.L. Sandell, Retinoic acid regulates embryonic development of mammalian submandibular salivary glands, Dev. Biol. 40 (1) (2015) 57–67.
[41] I.M. Lombaert, S.M. Knox, M.P. Hoffman, Salivary gland progenitor cell biology provides a rationale for therapeutic salivary gland regeneration, Oral Dis. 17 (5) (2011) 445–449.
[42] J. Jung, J.W. Kim, H.J. Moon, J.Y. Hong, J.K. Hyun, Characterization of neurogenic potential of dental pulp stem cells cultured in xeno/serum-free condition: in vitro and in vivo assessment, Stem Cell. Int. 2016 (2016), 6921097.
[43] J.N.A. Ferreira, C. Zheng, I.M.A. Lombaert, C.M. Goldsmith, A.P. Cotrim, J.M. Symonds, V.N. Patel, M.P. Hoffman, Neurturin gene therapy protects parasympathetic function to prevent irradiation-induced murine salivary gland hypofunction, Mol. Ther. Meth. Clin. Dev. 9 (2018) 172–180.
[44] W. Martens, E. Wolfs, T. Struys, C. Politis, A. Bronckaers, I. Lambrichts, Expression pattern of basal markers in human dental pulp stem cells and tissue, Cells Tissues Organs 196 (6) (2012) 490–500.
[45] V. Tirino, F. Paino, A. De Rosa, G. Papaccio, Identification, isolation,

characterization, and banking of human dental pulp stem cells, Meth. Mol. Biol. 879 (2012) 443–463.
[46] L. Lu, Y. Li, M. Du, C. Zhang, X. Zhang, H. Tong, L. Liu, T. Han, W. Li, L. Yan, N. Yin, H. Li, Z. Zhao, Characterization of a self-renewing and multi-potent cell population isolated from human minor salivary glands, Sci. Rep. 5 (2015).
[47] J. Feng, M. van der Zwaag, M.A. Stokman, R. van Os, R.P. Coppes, Isolation and characterization of human salivary gland cells for stem cell transplantation to reduce radiation-induced hyposalivation, Radiother. Oncol. 92 (3) (2009) 466–471.
[48] A. Sato, K. Okumura, S. Matsumoto, K. Hattori, S. Hattori, M. Shinohara, F. Endo, Isolation, tissue localization, and cellular characterization of progenitors derived from adult human salivary glands, Clon Stem Cell 9 (2) (2007) 191–205.
[49] L.S. Nanduri, M. Baanstra, H. Faber, C. Rocchi, E. Zwart, G. de Haan, R. van Os, R.P. Coppes, Purification and ex vivo expansion of fully functional salivary gland stem cells, Stem Cell Rep. 3 (6) (2014) 957–964.
[50] S.M. Knox, I.M. Lombaert, C.L. Haddox, S.R. Abrams, A. Cotrim, A.J. Wilson, M.P. Hoffman, Parasympathetic stimulation improves epithelial organ regeneration, Nat. Commun. 4 (2013) 1494.
[51] J.K. Placone, A.J. Engler, Recent advances in extrusion-based 3D printing for biomedical applications, Adv. Healthc. Mater. 7 (8) (2018), e1701161.
[52] V.N. Patel, I.T. Rebustini, M.P. Hoffman, Salivary gland branching morphogenesis, Differentiation 74 (7) (2006) 349–364.
[53] T. Jaskoll, G. Abichaker, D. Witcher, F.G. Sala, S. Bellusci, M.K. Hajihosseini, M. Melnick, FGF10/FGFR2b signaling plays essential roles during in vivo embryonic submandibular salivary gland morphogenesis, BMC Dev. Biol. 5 (2005) 11.
[54] M. Entesarian, H. Matsson, J. Klar, B. Bergendal, L. Olson, R. Arakaki, Y. Hayashi, H. Ohuchi, B. Falahat, A.I. Bolstad, R. Jonsson, M. Wahren-Herlenius, N. Dahl, Mutations in the gene encoding fibroblast growth factor 10 are associated with aplasia of lacrimal and salivary glands, Nat. Genet. 37 (2) (2005) 125–127.
[55] Y. Yamamura, H. Yamada, T. Sakurai, F. Ide, H. Inoue, T. Muramatsu, K. Mishima, Y. Hamada, I. Saito, Treatment of salivary gland hypofunction by transplantation with dental pulp cells, Arch. Oral Biol. 58 (8) (2013) 935–942.